Potential of ligand-promoted dissolution at mild pH for the selective recovery of rare earth elements in bauxite residue

Claire Lallemand, Jean-Paul Ambrosi, Daniel Borschneck, Bernard Angeletti, Perrine Chaurand, Andrea Campos, Morgane Desmau, Till Fehlauer, Melanie Auffan, Jérôme Labille, et al.

Potential of ligand-promoted dissolution at mild pH for the selective recovery of rare earth elements in bauxite residue

Claire Lallemand[†], Jean Paul Ambrosi[†], Daniel Borschneck[†,O], Bernard Angeletti[†,O], Perrine Chaurand[†,O], Andrea Campos[‡], Morgane Desmau[§], Till Fehlauer[†], Mélanie Auffan[†,^] Jérôme Labille[†], Nicolas Roche[†,▽], Laurent Poizat[‖], Blanche Collin[†,O], Jérôme Rose[†,^], Clément Levard[†,O]

[†]*Aix Marseille Univ, CNRS, IRD, INRAE, CEREGE, Aix-en-Provence 13545, France*

[‡]*Aix Marseille Univ, CNRS, Centrale Marseille, FSCM (FR1739), CP2M, 13397 Marseille, France*

§ Deutsches Elektronen-Synchrotron DESY 22607, Hamburg, Germany

[^]*Duke university, Civil and Environmental Engineering department, Durham, USA*

[‖]*Alteo Environnement, Gardanne, France*

[▽]*INternational Water Research Institute (IWRI), Mohammed VI Polytechnic University, Ben Guerir 43150, Morocco*

[O]*Laboratoire Mixte International Activité Minière Responsable "LMI-AMIR", IRD/UM5/INAU, 10000 Rabat, Morocco*

Jean Paul Ambrosi : ambrosi@cerege.fr
Daniel Borschneck : borschneck@cerege.fr
Bernard Angeletti : angeletti@cerege.fr
Perrine Chaurand : chaurand@cerege.fr
Andrea Campos : andrea.campos@univ-amu.fr
Morgane Desmau : morgane.desmau@gmail.com
Till Fehlauer : fehlauer@cerege.fr
Mélanie Auffan : auffan@cerege.fr
Jérôme Labille : labille@cerege.fr
Nicolas Roche : roche@cerege.fr
Laurent Poizat : Laurent.POIZAT@alteo-alumina.com
Blanche Collin : collin@cerege.fr
Jérôme Rose : rose@cerege.fr
Clément Levard : levard@cerege.fr

Key words: Bauxite Residue (BR); Circular Economy; Rare Earth Elements (REEs); Low Molecular Weight Organic Acids (LMWOAs); Ligand-promoted Dissolution; Characterization, Critical Elements, Speciation.

Abstract

In a context of overexploitation of natural resources, a circular economy and particularly the extraction of resources from secondary sources, are essential to sustain a number of key technologies including renewable energies. Among secondary sources, bauxite residue contains critical elements including rare earth elements (REEs) (712mg/kg). We investigated the use of soft and selective dissolution protocols at mild pHs (2-6) as an alternative to pyro- and hydrometallurgy for the recovery of REEs through ligand-promoted dissolution. This approach depends on the detailed characterization of the waste and the speciation of targeted elements. We assessed dissolution using low molecular weight organic acids (LMWOAs) and their conjugate bases. Citric acid/citrate showed satisfactory dissolution of REEs (up to 50% of light REEs) up to a pH of nearly 5, while tartaric acid/tartrate showed the best dissolution selectivity (enrichment factor up to 21.5 compared to Fe, Al and Ti). Almost no heavy REEs were dissolved in any of the conditions tested, probably due to the high chemical stability of their bearing phases. Indeed, heavy REEs were found as discrete phosphate particles.

Synopsis

Ligand-promoted dissolution, an interesting mechanism for the development of selective recovery processes of REEs from bauxite residue in mild pH conditions.

Introduction

The world population has increased fivefold since the 1900s, leading to overexploitation of the Earth's primary resources. Metals are one of these resources, particularly the critical metals used in modern technologies (smartphones, electronic compounds, wind turbines, permanent magnet, electric cars, etc.) because of their unique physical and chemical properties[1].These critical elements combine high economic value (in terms of end-use applications) and high risk of disruption in supplies due to limited reserves and geopolitical considerations [2,3].

Among these metals, rare earth elements (REEs), including lanthanides, yttrium (Y) and scandium (Sc), are among the most critical in Europe. Global consumption increased from 80 000 tons of rare earth oxides in 2000 to 140 000 tons in 2019[1]. REEs are often separated into two subgroups according to their different physico-chemical properties: La, Ce, Pr, Nd, Sm, Eu and Gd are classified as light rare earth elements (LREEs) and Tb, Dy, Ho, Er, Tm, Yb, and Lu are classified as heavy rare earth elements (HREEs). Yttrium and Sc are often included in the REE group because of their similar physico-chemical properties. Although Sc often behaves differently than other REEs, partly due to its smaller radius (for example, it can replace iron in goethite [4]). Yttrium behavior is very similar to that of HREEs (similar ionic radii and valence state).

Most REEs are produced in China, which accounts for 86% of world production (average 2012-2016, EU report 2020), and is also the world's largest consumer and exporter [5]. REEs are almost entirely produced by extraction from natural ores, mostly using controversial methods with negative sanitary (radioactivity, corrosivity) and environmental impacts (water/soil contamination) [6]. This mining industry is also a particularly big consumer of energy, water, and chemicals, and produces effluents and solid wastes that are intentionally or accidentally released into the environment [6]. In this context, there is an urgent need to find alternatives for the production of REEs to reduce (i) the supply risk and (ii) the environmental and sanitary impacts associated with their extraction.

In circular economy, mining and industrial wastes represent secondary REE resources that are largely under-exploited partly because of the low cost of extracting REEs from natural ores and the lesser quality of secondary sources compared to natural ones. However, given the strong pressure on these metals, mining secondary sources may become a sustainable source of REEs in the near future. Among secondary sources, bauxite residues (BR), also known as red mud when hydrated, are an attractive source of REEs. BR is an industrial waste resulting

from the extraction of alumina from natural bauxite rocks using the Bayer process (soda leaching). For example, a Jamaican residue contains up to 2,500 mg/kg of REEs [7] which is about 10 times higher than the natural abundance of REEs in the Earth's crust [8]. Extracting REEs from BR is a real economic and environmental challenge. Existing processes, usually based on the leaching of REEs from BR, use strong mineral acids such as hydrochloric, nitric, or sulfuric acids [9,10]. During acidification, proton-promoted dissolution digests most of the matrix with poor REE selectivity, requires post-leaching purification steps, and produces large quantities of hazardous acidic liquid and solid wastes.

The use of low molecular weight organic acids (LMWOAs) as alternatives to the strong acids traditionally used in hydro- or pyro-metallurgy, has been less studied, partly due to their lower leaching efficiency. Leaching efficiency reported in the literature using LMWOAs rarely exceeds 50% for LREEs and 65% for HREEs [11,12] (*see S1 in SI*) whereas strong acids usually dissolve 80-90% of REEs [13]. However, although less efficient, leaching with LMWOAs involving ligand-promoted dissolution has other advantages that deserve more attention with a view to designing more sustainable extraction strategies. In particular, ligand-promoted dissolution is expected to be more selective (i.e., to require fewer extraction steps and to produce less waste) and can be performed at more neutral pH (hence producing non-acidic solid and liquid wastes). However, developing such processes requires a better understanding of the speciation of the REEs, the identification of the bearing phases in the matrix, which we investigate here. In particular, ligand-promoted dissolution depends to a great extent on the specific affinity of LMWOAs for the surface of minerals and for the element in solution, which will be strongly affected by pH.

The aim of our study was to investigate the potential of ligand-promoted dissolution for the selective leaching of REEs in BR in mild conditions. We performed multi-scale characterization of the BR including the speciation of REEs (chemical composition, mineralogy, particle size, elemental distribution, speciation), and assessed the effects of a number of experimental variables including the nature of the LMWOAs and pH on dissolution efficiency and selectivity. For the first time, speciation of HREEs in bauxite residue has been described at the bulk scale and pH-dependent dissolution behavior has been reported. In light of these results, ligand-promoted dissolution mechanisms are discussed with a view to improving dissolution selectivity and yield in future work.

Material and methods

Material

The BR we studied came from Bouc-Bel-Air (South of France). It was produced and collected in February 2019 and stored in sealed plastic containers at ambient temperature until required. The fresh BR was sampled immediately after the chemical extraction of alumina (Bayer process) from bauxite, a lateritic deposit, originating from Guinea (West Africa). Before the experiments, the BR was dried at 60-70 °C for 2 days, manually ground in an agate mortar, sieved to 125µm and homogenized using an orbital shaker before use. The effect of different BR grinding methods on dissolution efficiency was further studied and is presented in SI (*see S2 in SI*)

Characterization of the bauxite residue

Chemical composition. Four samples of the same dry and ground BR were mineralized using the alkaline fusion method: 100 mg of BR and 500 mg of dry lithium tetraborate (flux) were mixed and heated at 1 000 °C in an oven. The resulting fusion bead was dissolved in 40ml of nitric acid (1N). The final solutions were diluted in 2% nitric acid at a dilution factor of 200 and trace elements and minor elements including REEs were analyzed with a Perkin Helmer 300X quadrupole ICP-MS for, while major elements were analyzed with a Perkin Elmer ICP-OES Optima 4300 DV. The results (concentration in mg/kg) are expressed along with the average and the standard deviation of the 4 samples.

Mineralogy of the bauxite residue. X-Ray diffraction was performed at 40 kV and 40mA on a Panalytical X'Pert Pro θ-θ diffractometer equipped with a rear monochromator and a cobalt anticathode (K_α = 1.79Å). Scans were made between 5° and 75° (2θ) with a step size of 0.033°. The sample was rotated at 15 rpm during analysis to improve the statistics.

Spatial distribution of REEs. Scanning electron microscopy coupled with EDX analysis (SEM-EDX) and Nano X-Ray Fluorescence (Nano-XRF) microscopy were performed to assess the spatial distribution of the REEs in the BR. For the SEM-EDX analysis, a BR pellet was prepared with 5g of BR dispersed in 25mL of ultrapure water, centrifuged at 2061xg for 15 minutes and dried to remove excess salts. The process was repeated 3 times. SEM was carried out at 30kV using a Zeiss GeminiSEM 500 SEM equipped with an EDAX Octane Silicon Drift Detector (129 eV energy resolution for Manganese) at Aix-Marseille University.
Nano X-Ray Fluorescence microscopy (nano-XRF) experiments were performed at the Nanoscopium hard X-ray nanoprobe beamline of Soleil Synchrotron (Saint-Aubin, France).

Dry and washed BR was homogeneously dispersed on Kapton tape for analysis. The monochromatic X-ray beam energy was set at 18.3keV with a gap size of 150 x 60nm, focused with a Kirckpatrick-Baez nano-focusing mirror. A fast continuous scanning technique was used to obtain elemental mapping with an integration time of 40ms per pixel. Y was located at the nano scale with the fluorescence K-emission line at 14.9 keV. A dead time correction was applied to each pixel. Elemental maps were extracted from the hyperspectral maps, including Y (K_α 14.96 keV), Fe (K_α 6.40 keV), Ti (K_α 4.51 keV), Yb (L_α 7.42 keV) and Er (L_β 7.81 keV). Elemental mapping was performed by selecting an ROI of energy centered on the emission line on the XRF spectra using PYMCA software (background subtraction, calibration, fit (*see S3 in SI*)). Possible correlations were further investigated by calculating the Pearson coefficient on the nano-XRF maps.

Yttrium speciation. X-ray absorption spectra (XAS) at Y K-edge (17.038 keV) were recorded by the P65 undulator beamline at the Deutsches Elektronen-Synchrotron (Hamburg, Germany). Incoming photon flux energy was modulated using a Si(111) double crystal monochomator and higher harmonics were suppressed using Rh-plane mirrors. The data were collected in continuous mode with a beam size of 0.3×1.5 mm^2. Samples were prepared as pure pellets (50mg) for BR, or as diluted pellets with polyvinylpyrrolidone for model compounds. For the latter, the quantity of the sample was calculated to get $\Delta\mu_{theorical}$=1. Each spectrum was measured at 20K to prevent beam damage. The BR sample was measured in fluorescence mode with a Hitachi/Vortex 4-pixel silicon drift detector (SDD), One spectrum represented an average of 3 to 6 scans of Y reference compounds and 30 scans of the BR sample, depending on the concentration of Y and the noise level. Energy was calibrated using reference Y metal foil. E0 (absorption edge) was defined at 17038eV at the gap between the two maximum points of the first derivative. Calibration, normalization and averaging data were performed using Athena software [14].

A library of Y reference compound spectra was used to identify Y species in BR. It consisted in commercial references: yttrium oxide (Y_2O_3; Acros Organics), yttrium carbonate ($Y(CO_3)_3.xH_2O$; Alfa Aesar), natural minerals (xenotime, YPO_4), and model compounds synthesized in the laboratory (crystallized and amorphous Y phosphates, Y hydroxide, Y-adsorbed on montmorillonite, (*see S4 in SI for synthesis protocols*). Least square linear combination fitting (LCF) of the XANES (X-ray Absorption Near Edge Spectroscopy) region was performed over an energy range of -50eV to +200eV around E0 using Athena software. The residual factor of LCF was calculated as follows: $R = (\Sigma(\mu_{exp} - \mu_{fit})^2)/\Sigma(\mu_{exp})^2$ using Athena software. At each step of the fitting, an additional reference spectrum was added if the

two following conditions were true: the R factor decreased by 20% or more and the additional reference contributed 10% or more Y species. The uncertainty of this LCF method was estimated at ±15% [15].

Dissolution with LWMOAs. Three LMWOAs (citric, tartaric, and oxalic acids) and their conjugated bases were tested. The molecular structures of LMWOAs are similar with a short carbon chain (C_2-C_6), carboxylic acid functions (-COOH) and similar pKa. The complexing reagents used were citric acid (>99%), di-hydrated trisodium citrate (99%), di-hydrated oxalic acid (98%), mono-hydrated di-ammonium oxalate (>99%), L (+)-tartaric acid (99.5%), and tetra-hydrated potassium tartrate (<99%). The dissolution experiments consisted in two 48-h sequential experiments performed in triplicate at a liquid/solid ratio (L/S) of 50 (0.8g of dried and hand-ground BR in 40ml of complexing solution at 0.1mol/L). Forty-eight hours consist in the time needed to reach a steady-state dissolution for most elements (*see S5 in SI*). The complexing solution was renewed 48 hours after the solid phase was separated by centrifugation (6 133 x g). To increase the pH from 2 to 9, the organic acids used were mixed with their conjugated base at different ratios (citric acid and citrate for example, (*see S6 in SI*)). The total concentration of complexing reagents (LMWOAs and their conjugate base) was maintained at 0.1M. During dissolution, the solutions were stirred on a Heidolph REAX 20 1-16 RPM mechanical rotary shaker (14 rpm), at room temperature. pH was measured regularly with a HI 2550 Multiparameter pH/ORP/°C/EC/TDS/NaCl Bench Meter. In the literature (*see S1 in SI*), leachate is typically separated from the solid residue using 0.22µm or 0.45µm filters. Here, ultrafiltration (3kDa=1-2nm) of the leachate insured that there were no suspended particles in the solution by separating only dissolved species or small organic-metal complexes. The filtered solutions were diluted by a factor of 20 or 40 and analyzed using both ICP-OES and ICP-MS.

The results are presented with their dissolution percentage (concentration of the dissolved element in mg/kg divided by the concentration in the BR in mg/kg, converted into percentage). Selectivity was calculated with the enrichment factor (EF) according to the following equation:

$$EF = \frac{\frac{\sum[REEs]\,(dissolved)}{\sum[Fe,Al,Ti]\,(dissolved)}}{\frac{\sum[REEs](BR)}{\sum[Fe,Al,Ti](BR)}} \quad \text{(Equation 1)}$$

Where *dissolved* stands for the concentrations of element in the filtered solution (mg/kg) and *BR* for the concentrations of the element in the original material (mg/kg). EF stands for the enrichment of REEs, Y and Sc in the 3 most concentrated elements (Fe, Al, Ti) in BR.

Dissolution with nitric acid. A dissolution experiment with a mineral acid was performed for comparison with ligand-promoted dissolution. Two concentrations of HNO_3 (0.1M, 0.05M) were used to target low and close to neutral pH (pH_{mix}=2 and 5.3 respectively). The dissolution protocol used was the same as that used for dissolution with LMWOAs described above.

Results and discussion

Characterization of initial BR

Chemical composition and mineralogy

The chemical composition and the mineralogy of BR is presented in *Table 1* and in SI (*S7*)**.** BR was mainly composed of Fe (33wt%), in the form of hematite (α-Fe_2O_3) and goethite (α-FeOOH) followed by Ti (5.41wt%) as rutile (TiO_2) and Al (3.91wt%) as gibbsite ($Al(OH)_3$). Calcium is present as calcite ($CaCO_3$). Two silicate phases were identified: cancrinite ($Na_6Ca_2CO_3$, $Al_6Si_6O_{24}.2H_2O$) and katoite ($Ca_3Al_2(SiO_4)_{3-x}(OH)_{4x}$, x=1.5 to 3). This is consistent with the literature on BR composition and mineralogy: Fe and Al are usually the two main concentrated elements, but their concentration varies considerably depending on the origin, the type of the bauxite (lateritic or karstic) [7,16], the Al extraction treatment conditions (pH, temperature, reagents) and the storage time [17,18]. Together, reviews[17,19,20] by *Xue et al. 2016, Gräfe, Power, and Klauber 2011* and *Snars and Gilkes 2009*, and the estimation by the *International Aluminum Institute* (IAl) and the *European Aluminum Association (EAA)* in 2014, suggest that Fe_2O_3 comprises from 7% to 72wt% of the residue, Al_2O_3 2% to 33wt%, TiO_2 1% to 23 wt%, CaO 0% to 14 wt% and SiO_2 5% to 30 wt%. Aside from Al and Fe, the mineralogy we observed is consistent with the literature[17]. Other inorganic phases reported in other studies including perovskite ($CaTiO_3$), sodalite ($Na_4(Si_3Al_3)O_{12}Cl$), diaspore (AlO(OH)) or magnetite (Fe_3O_4) were not detected in our BR sample [21,22].

The total amount of REEs, including Y and Sc in the BR studied here was 712.6mg/kg. The most concentrated REEs were Ce (220.7mg/kg), Y (121.2mg/kg), La (105.9mg/kg) and Sc (75.2mg/kg). The concentration of REEs in BR reported in the literature is highly variable (*see S8 in SI*). The main variations in the concentration of REEs are explained by the origin of the bauxite deposit: karstic-type bauxites (12% of the global bauxite deposits mostly located in Europe) are usually richer in REEs than lateritic-type bauxites (88% of the global bauxite that can be found in Guinea, India or Australia for example). In this study, the BR was

produced from a lateritic deposit (in Guinea, West Africa) using the Bayer process. No particular anomalies were observed according to the PAAS-normalized REE pattern (*see S9 in SI*).

Table 1 : Chemical composition of the BR for REEs, Sc, Y, and major elements (average ± standard deviation). Concentrations in the Earth's crust were taken from Kabata-Pendias 2011.

REEs	BR Concentration (mg/kg DW)	Earth's crust (mg/kg DW)
Sc	75.2±1.7	16-30
La	105.9±2.0	30
Ce	220.7±3.2	60
Pr	21.0±0.3	8.2
Nd	72.1±0.9	28
Sm	16.7±0.2	4.7
Eu	3.1±0.1	1.2
Gd	16.7±0.2	5.4
Tb	3.1±0.1	0.6
Dy	21.3±0.4	3.7
Ho	4.6±0.1	0.8
Er	14.4±0.5	2.8
Tm	2.2±0.1	0.5
Yb	15.2±0.3	2.2
Lu	2.3±0.1	0.3
Y	121.2±3.0	20-33
Total REEs	***712.6±13.1***	*168-200*

Majors	Mass (%)	Equivalent oxide (%)
Fe	33.03±0.61	47.22±0.87 (Fe_2O_3)
Ti	5.41±0.05	9.02±0.08 (TiO_2)
Al	3.91±0.23	7.39±0.43 (Al_2O_3)
Ca	2.95±0.20	4.13±0.28 (CaO)
Si	1.43±0.12	3.06±0.26 (SiO_2)
P	0.17±0.02	0.77±0.07 (PO_4)

Spatial distribution of REEs in BR

Elemental mapping with SEM-EDX confirmed the prevalence of Fe in our BR matrix (*Figure 1A*). Discrete particles rich in Al (dark blue), Si (red), Ti (pink) and Ca (cyan) were also observed confirming the results of bulk analysis and the mineralogy observed by XRD. The

detection of REEs was very challenging because of (i) their relatively low concentration (especially HREEs), and (ii) the overlap between their L_α fluorescence emission lines with the K_α emission lines of Ti, Cr and Fe (regarding LREEs). However, few Y-rich particles (white) were observed with SEM-EDX (*Figure 1A*). Y was not correlated with Al, Fe, Ti, Si and Ca but co-localized with P (light blue). This co-localization raises the hypothesis that Y and P could exist as yttrium phosphates (YPO_4). Indeed, Y commonly occurs in phosphate minerals (such as monazite, xenotime) in nature and forms very stable phases. At this stage, no other REEs were detected by SEM-EDX.

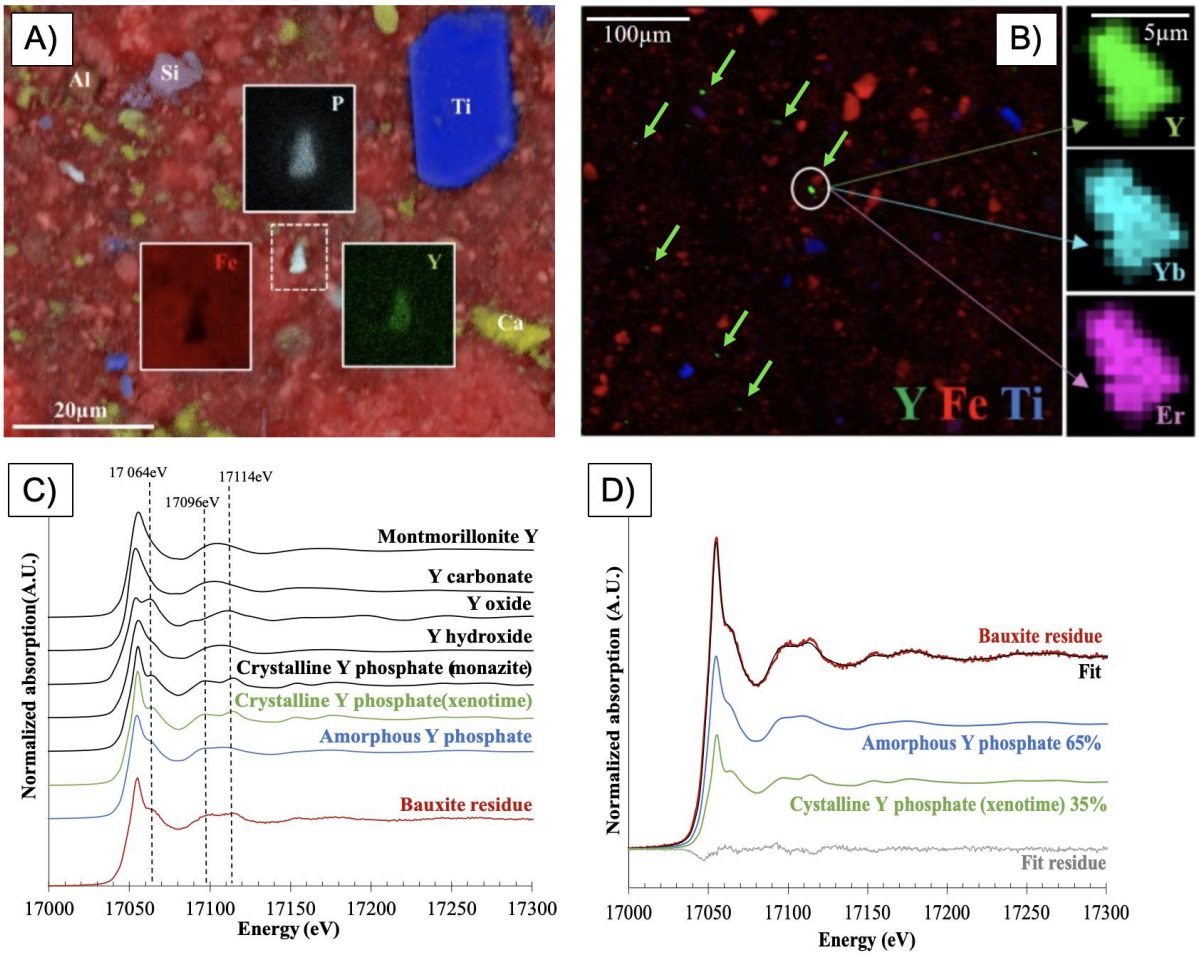

Figure 1: (A) Combined elemental map obtained by SEM-EDX showing the spatial correlation between Al, Si, Ti, Fe, Ca, Y and P in BR sample (30kV, pixel=71.11nm). (B) Combined elemental map obtained by nano-XRF showing the distribution of Fe, Ti, Y Yb, Er in BR sample, (1px = 1µm for the large image, 1px = 400nm for small images). (C) Bulk XANES spectra of BR and model compounds at the Y K-edge and (D) LCF performed with Athena software (R-factor=0.0009)(right).

Deeper investigation of the spatial distribution was performed at the SOLEIL synchrotron with using nano-XRF which is more sensitive than that of SEM-EDX. In agreement with SEM, nano-XRF revealed several Y-rich particles (*Figure 1B*) of 4.9±1.9µm (n=24) not associated with major elements (Fe, Ti, Al, Si, Ca) but co-localized with other REEs, especially HREEs, as expected (Gd, Er, Yb). LREEs (La, Ce, Nd) were also investigated but were not detected, probably because their signals are hidden by the intense XRF emissions of Ti, Cr and Fe. P was not detected either because of the limited sensitivity of the beamline for the detection of P Kα emission lines. At this low energy (2.01keV), fluorescence signal is strongly absorbed by the air before reaching the detector, unlike in SEM-EDX analysis, which is performed under vacuum.

The Pearson coefficient was calculated for some trace elements (Y, Yb, Gd, Er, Cu, U, Th) and for major elements (Fe, Ti) on the Y-rich area (Inset in *Figure 1B***)** (*Figure S2*, *SI*). A correlation was observed (Coef≥0.70) for the HREEs (Gd, Er, Yb) and Y, but also for other elements of interest present at low concentrations such as Cu, U and Th. Fe and Ti were not correlated with these elements. To confirm our hypothesis that Y forms YPO_4 phases, probably associated with HREEs in BR, Y speciation was investigated at the bulk scale.

Y speciation in BR

The bulk XAS spectrum (*Figure 1C*) obtained for the BR sample closely resembled spectra corresponding to synthesized Y phosphates (amorphous and crystallized monazite), and xenotime (natural and crystalline phosphate mineral). The spectra of these model compounds were characterized by specific features, i.e., a shoulder at 17064eV in the white line and the 2 features at 17096eV and 17114eV. The amorphous Y phosphate had less pronounced features. Linear combination fitting (LCF) confirmed that the Y speciation in BR was YPO_4 (*Figure 1D*) in agreement with the Y/P spatial correlation previously identified with SEM-EDX. The best fit was obtained using a mixture of crystalline and amorphous YPO_4 (35% xenotime and 65% amorphous).

These results concerning HREEs are consistent with those obtained in the study by *Vind and al. (2018)*[16] where Y, Gd, Dy and Er were found to be co-localized at the particle scale using an Electron Probe Micro Analyzer (EPMA) and EDX methods as xenotime/churchite-kind phases (yttrium phosphate). Observed in a karstic BR, these microscale particles were slightly smaller (2-3µm) than the ones observed in our study. Our study thus confirms for the first time at the bulk scale, observations performed at small scale. It is likely that we only observed the biggest particles and missed a large fraction of sub-micron particles, potentially amorphous (1µm pixel

on the big map in *Figure 1B*). The distributions of REEs and Y observed here as well as by *Vind and al. (2018)* [16] confirm that BR is potentially an ideal matrix for developing selective dissolution of HREEs since it is concentrated in accessible particles and not associated with major elements.

Dissolution of REEs using LWMOAs

Ligand-dependent dissolution

It has been shown that aliphatic acids (citric acid, oxalic acid, succinic acid, malic acid, etc.) produced by organisms such as plants, fungi and bacteria are good candidates for the recovery of REEs from REEs/Y-rich phosphate minerals (apatite and monazite), particularly citric acid [23–25]. Some of these organic acids have also been identified in the literature as biomolecules capable of selectively solubilizing REEs from BR (*Table S1, SI*).

Figure 2 shows the fraction of dissolved elements (REEs, Y, Sc and major elements Al, Ti, Fe) after two-step sequential extraction (2x48 h) for three organic acids that have known affinity for REEs (citric, tartaric, and oxalic acids) and nitric acid. Citric and tartaric acids exhibit quite similar behavior that is very different from that of oxalic acid. Citric acid dissolves more LREEs and Al. It can extract up to 49% of LREEs and 12% of HREEs. Tartaric acid dissolves slightly more HREEs, Y, Sc, Ti and Fe. More interestingly, it dissolves Al poorly in comparison with citric acid, which might be of interest in terms of selectivity. This can be explained by the lower affinity of tartrate for Al compared to citrate (log K= 5.32 and 7.98 respectively). Finally, no REEs were measured in solution in the oxalic acid experiment, unlike Al, Ti, Sc, and a small amount of Fe. This was not surprising since oxalic acid is often used in industrial processes to precipitate the REEs as insoluble metal-oxalate complexes [26–29]. In our study, it was not possible to quantify the amount of REEs that reacted with oxalic acid.

In the citric and tartaric acid systems, LREEs (La to Sm) were better dissolved than HREEs (Ho to Lu, Y and Sc) and the dissolution of Eu to Dy was intermediate. Two hypotheses may explain this trend: (i) the stability constants of ligand-REEs complexes are lower for HREEs than for LREEs for a given speciation, (ii) LREEs and HREEs have different speciation and consequently different affinities for the extractant. The second hypothesis is more likely, in view of the speciation data collected in our study and in the study by *Vind and al. (2018)*[16]. In addition, stability constants reported in the literature show either a continuous increase with Z or close values for LREEs and HREEs (*see S10 in SI*) [30,31], which is not consistent with our first hypothesis.

For the sake of comparison, a similar experiment was performed using nitric acid. Nitric acid is usually described in the literature as one of the most efficient inorganic lixiviants for leaching of REEs from BR under very acidic conditions (pH<0.5) [10,11,32]. At pH 1.9±0.8 (0.1M HNO_3), the recovery yields were slightly lower but close to those obtained with citric and tartaric acids at pH=2.5±0.4 and 2.6±0.4. We hypothesize that at these relatively low pH, proton-promoted dissolution is the dominant mechanism for the dissolution of REEs. However, in the presence of LMWOAs, ligand-promoted dissolution is also probably involved in the dissolution of LREEs, which may explain the slightly better dissolution efficiency of REEs by citric and tartaric acids compared to HNO_3 treatment. However, at this stage, it is difficult to dissociate the two mechanisms taking place with LMWOAs. The potential effect of the ligand-promoted dissolution was studied by performing similar experiments at higher pH at which proton-promoted dissolution is negligible.

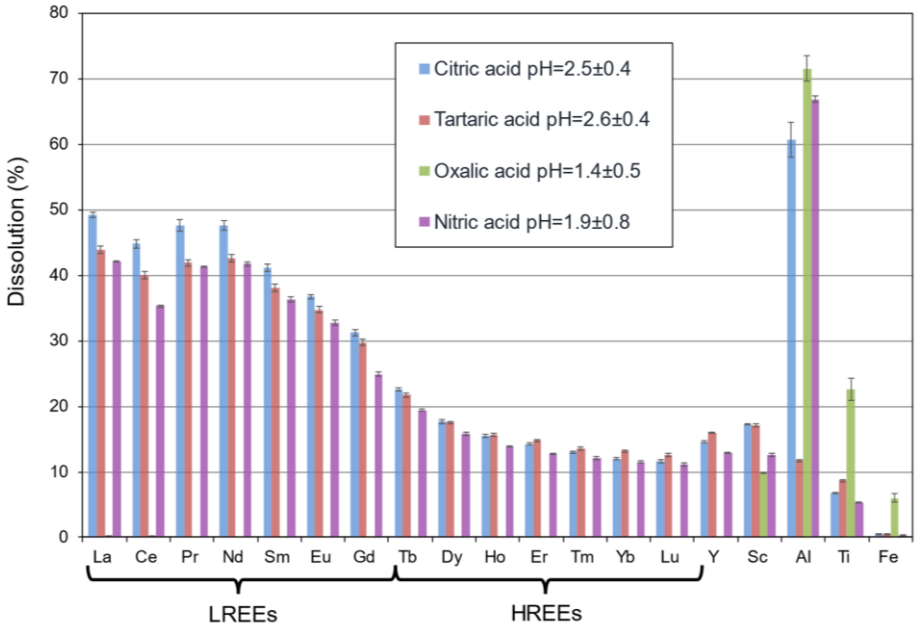

Figure 2 : Dissolution of REEs, Fe, Al and Ti with citric acid, tartaric acid, oxalic acid, and nitric acid (2x48 h, 0.1mol/L, L/S=50).

pH-dependent dissolution

To further decipher the role of ligand-promoted dissolution, a set of dissolution experiments was performed at different pH. pH was controlled by varying the acid/conjugate base ratio.

The better dissolution of LREEs compared to HREEs observed above at pH 2.5 with citric acid and at 2.6 with tartaric acid was also observed at all the pH tested using the citric acid/citrate and tartaric acid/tartrate systems.

Regarding the citric acid/citrate system, similar dissolution was obtained from pH 2.5 to 4.7 before a significant drop at pH 6 (*Figure 3A*). The average dissolution of Al is 61%, with low variability among the pH range investigated here. Ti and Fe dissolution were low (%Ti<6%, %Fe<1%) and decreased toward alkaline pH.

The tartaric acid/tartrate system behaved differently from the citric acid/citrate system with a decrease in the dissolution of REEs with increasing pH (*Figure 3B*). However, the major elements including Al were poorly dissolved compared to in the citric acid/citrate system. Al dissolution did not exceed 12% (pH=2.6±0.4), only 9% of Ti, and less than 0.5% of Fe were dissolved.

As mentioned earlier, oxalic acid is known in the literature as an efficient complexing and precipitating agent for REEs at acidic pH [26–29]. Consequently, no REEs or Y dissolution was measured (*Figure 3C*) regardless of the pH in the oxalic acid/oxalate system (%REE,Y<0.5%). A fraction of REEs probably precipitated with oxalate and was therefore not detected in the supernatant. Interestingly, Sc was partly dissolved with optimal extraction at pH=5.1±1.6 (%Sc=18%) which confirms the difference in the chemical behavior of this element from that of other REEs. Between 60% and 70% of the Al was dissolved at pH< 7.5 and Ti dissolution increased from 13% at pH=5.1±1.6 to 22% at pH=1.4. More Fe was more dissolved with oxalic acid than with the other organic ligands (%Fe>3.5% for pH<2).

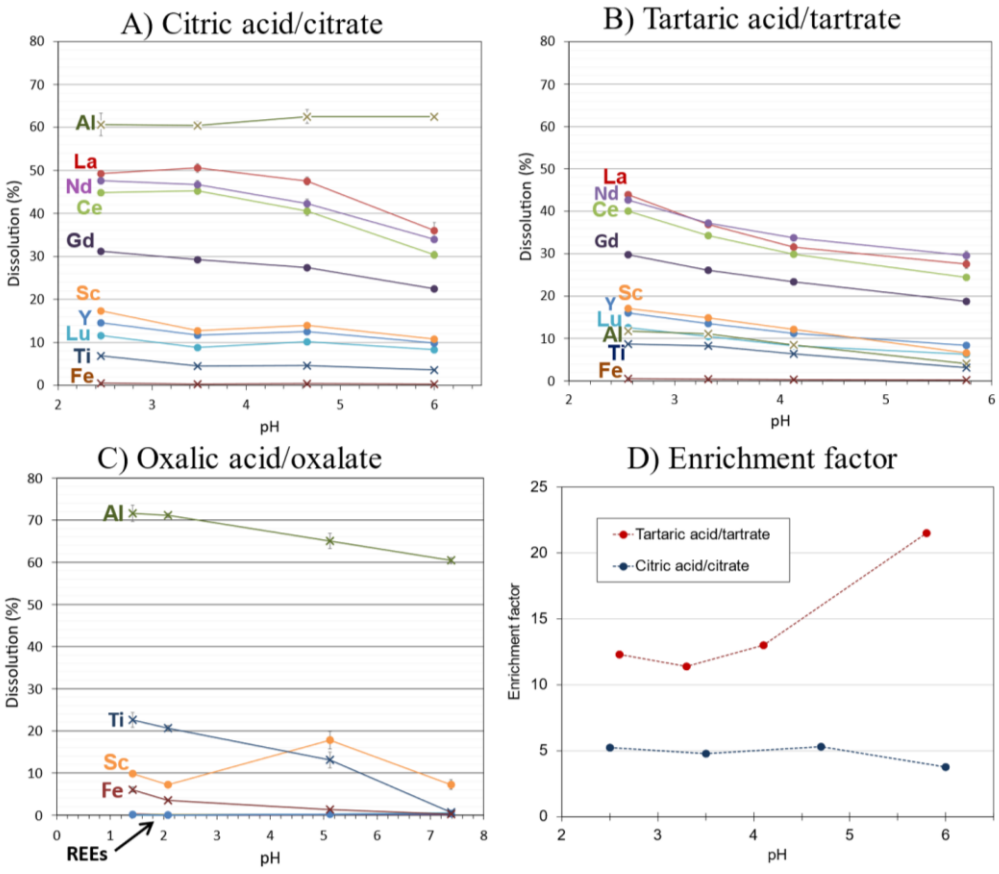

Figure 3 : Dissolution of REEs, Sc, Y, Al, Ti, and Fe with (A) citric acid/citrate, (B) tartaric acid/tartrate, and (C) oxalic acid/oxalate as a function of pH (2x48h, L/S=50, 0.1mol/L). (D) Selectivity (expressed by the enrichment factor) for the dissolution with citric acid/citrate and tartaric/tartrate acid.

Although less efficient at mild pH than the citric acid/citrate system, the tartaric acid/tartrate system is interesting in terms of selectivity, especially related to Al. To quantify the selectivity of REE dissolution, an enrichment factor (EF) towards the 3 main elements was calculated (*Figure 3D*). Despite slightly lower recovery yields, tartaric acid was found to be more selective for REEs than citric acid regardless of the pH: $EF_{citric\ acid}$=3.8 to 5.3 and $EF_{tartaric\ acid}$=11.4 to 21.5 for 2.5<pH<6. The enrichment factor was similar regardless of the pH, except at pH=6 for tartaric acid where selectivity reached maximum.

Dissolution mechanisms

To better understand the mechanisms involved as a function of pH, recovery yields were measured using HNO_3 at 0.05M to reach a pH of 5.3 (*see S11 in SI*). In this condition, there was no dissolution of REEs, Y or Sc unlike in the citric/citrate and tartaric/tartrate systems at similar pH. This experiment confirms that at such mild pH, ligand-promoted dissolution is the main driver of the dissolution of REEs.

Two routes for ligand-promoted dissolution may exist, as illustrated in *Figure 4*. Based on the observations we made in this study for HREEs, we hypothesize that HREEs are hosted in a phosphate matrix. LREEs on the other hand are suspected to be concentrated within particles with varying chemistries [16]. The first route (R1 in Figure 4) is controlled by (i) the dissolution of the REE-hosting mineral defined by the solubility product constant K_{sp} and (ii) the affinity of the dissolved species for the organic ligand defined by the complexation constant $K_{complexation}$. The complexation of free REE^{3+} ion by organic ligands will shift the first equilibrium towards dissolution of REE-hosting mineral.

The second route (R2 in Figure 4) is controlled by the affinity of the organic ligand for the surface of the REE-hosting mineral present in BR ($K_{adsorption}$) and its ability to weaken the bonds that bind surface atoms to the particle and that will eventually break to form a complex in solution.

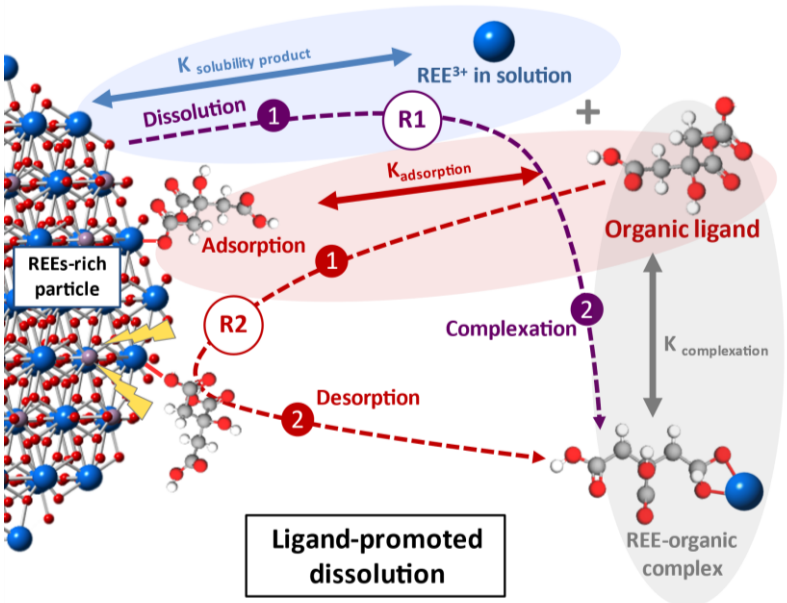

Figure 4 : Conceptual diagram of the chemical mechanisms involved in the dissolution of REEs in bauxite residues with organic ligands.

As a result of these processes, dissolution may be affected by a number of parameters including the solubility product of the different phases that comprise the BR, the affinity of the LMWOAs for soluble REEs and particle surfaces. For the latter, pH is a key parameter that controls the dissociation of LMWOA protons (pKa) and the surface charge of the mineral.

Therefore, improving dissolution efficiency requires a good understanding of dissolution mechanisms, which, in turn requires a good knowledge of the physico-chemical properties of the matrix. To give an example, the poor dissolution of HREEs in our case could be explained by their speciation. The REE-phosphates observed in our study are known to be very stable (poorly soluble, $K_{sp}=10^{-24.75}$ to $10^{-26.43}$ for REEs and Y)[33] which will limit dissolution (route 1) and prevent the release of the REE-organic ligand complex (route 2). Further improvement of the process for HREEs should focus on identifying other organic ligands that have a high affinity for phosphate minerals (either for the HREEs or for the phosphate function) in order to favor route 2 since route 1 seems unfavorable in the presence of REE-phosphate (*Figure 4*). The better dissolution yield of LREEs compared to HREEs was probably due to the occurrence of LREEs phases that are less chemically stable (e.g. higher solubility product (route 1) or less energetic release of REE-organic ligand complex (route 2)) than the HREEs-phosphates observed in our study. Although the speciation of LREEs seems to differ from that

of HREEs [16], the host LREEs-phases are still not known, and work is now underway to characterize it.

Conclusion

Rather than focusing on maximum dissolution efficiency, which is the primary objective of past studies on the dissolution of REEs from BR, our study aimed at investigating the potential of ligand-promoted dissolution for the selective dissolution of REEs under mild pHs. In the citric acid/citrate system, similar recovery yields were obtained at pH ranging from 2.5 to 4.7. Although slightly less efficient, the tartaric acid/tartrate system displayed interesting dissolution selectivity with enrichment factors comparable to those of Al, Fe and Ti reaching up to 21.5. Unlike in strong mineral acid, it is therefore possible to dissolve REEs at mild pH with relatively good selectivity.

Understanding ligand-promoted dissolution mechanisms in the optic of improving the efficiency and selectivity of REE dissolution requires a good knowledge of the BR matrix, which was investigated in our study. LREEs were recovered better than HREEs most probably because of the difference in speciation in the BR. Yttrium was found as 4.9 µm YPO_4 particles. HREEs co-localized with Y and, given the analogy between Y and HREEs, the latter probably form mixed phosphate phases. Although the formation of discrete particles of Y and HREEs appears favorable for selective dissolution, the very high chemical stability of these phosphate phases probably explains the poor recovery yields of Y and HREEs. LREE speciation is still not clear, although the literature reports LREEs (La, Ce, Nd) embedded in ferrotitanate phases, and minor amounts in carbonate and phosphate phases [16]. Despite measurement challenges, work is now underway to identify the LREE-bearing phases. In any case, we hypothesize that their speciation is more favorable for their recovery using LMWOAs. The case of Sc is probably not favorable for selective dissolution since it has been shown to be strongly associated with iron phases [4]. As an example, in a previous study, we showed that Sc can replace Fe in the goethite structure making dissolution selectivity impossible to address for this element [4].

Several options will be investigated in future studies to improve dissolution efficiency and selectivity, in particular for HREEs. One possibility is to favor route 2 of the mechanisms described in *Figure 4* by selecting appropriate organic ligands that have a stronger affinity for REE-rich phases than the LMWOAs tested in the present study. In this regard, understanding

the effect of ligand composition and structure (e.g. nature and number of functional groups, the presence of an hydroxyl group in α-, β- or γ-hydroxy acids, pKas, etc.) on the dissolution of REE-rich phases can help in the choice of more appropriate ligands in the optic of enhanced dissolution yield and selectivity. In addition, the use of organic molecules produced by living organisms will also be explored. It includes highly selective organic molecules produced specifically to recover REEs by methylotroph bacteria such as lanmodulin [34–36] but also other molecules produced by plants, bacteria or fungi than are known to dissolve phosphates and/or REEs in soil (siderophores [37–39], formic acid, succinic acid, malic acid, amino acids…) [23,25,40–46]. In this regard a better knowledge of plants and microorganisms developing in BR deposits may be particularly informative for selecting appropriate bio-inspired extraction strategies[47–49].

Although poorly investigated compared to conventional hydrometallurgy, we believe that selective dissolution using ligand-promoted dissolution is a promising approach for the design of sustainable extraction processes of various critical elements from a variety of secondary sources. In a circular economy, this approach makes it possible to decrease pressure on natural resources, to limit the number of extraction steps and to minimize the production of hazardous wastes.

Supplementary information: Complementary literature, additional experimental details including synthesis protocols, additional results including XRF spectra analysis, granulometry experiments and nitric acid dissolution. The document is available online.

Acknowledgments

The authors acknowledge financial support from the CNRS through the MITI interdisciplinary programs (PRIME 2020: ExtraMet project), the Agence Nationale de la Recherche through the RECALL project (ANR-20-CE04-0007). This work was supported by the TelluS Program of CNRS/INSU as well as in the framework of the OHM Bassin Minier de Provence and (co)funded by the LabEx DRIIHM, French program "*Investissements d'Avenir*" (ANR-11-LABX-0010) managed by the ANR. The thesis contract of C. Lallemand was funded by CEPAC (*Caisse d'épargne* Provence Alpes Corse) through the AMIDEX foundation (Aix-Marseille University). Synchrotron data were obtained on SOLEIL and DESY synchrotrons. We are very grateful to the SOLEIL beamline staff for their assistance, in particular to Andrea Somogyi (Nanoscopium). We also acknowledge DESY (Hamburg,

Germany), a member of the Helmholtz Association HGF, for the use of experimental facilities. Parts of this research were carried out at P65.

REFERENCES

(1) European Commission, Study on the EU's List of Critical Raw Materials - Final Report (2020).

(2) Jowitt, S. M.; Werner, T. T.; Weng, Z.; Mudd, G. M. Recycling of the Rare Earth Elements. *Current Opinion in Green and Sustainable Chemistry* **2018**, *13*, 1–7. https://doi.org/10.1016/j.cogsc.2018.02.008.

(3) *Environmental Technologies to Treat Rare Earth Elements Pollution: Principles and Engineering*; Sinharoy, A., Lens, P. N. L., Eds.; IWA Publishing, 2022. https://doi.org/10.2166/9781789062236.

(4) Levard, C.; Borschneck, D.; Grauby, O.; Rose, J.; Ambrosi, J.-P. Goethite, a Tailor-Made Host for the Critical Metal Scandium: The FexSc(1-x)OOH Solid Solution. *Geochem. Persp. Let.* **2018**, 16–20. https://doi.org/10.7185/geochemlet.1832.

(5) Mancheri, N. A. Effect of Chinese Policies on Rare Earth Supply Chain Resilience. **2019**, 12.

(6) Golev, A.; Scott, M.; Erskine, P. D.; Ali, S. H.; Ballantyne, G. R. Rare Earths Supply Chains: Current Status, Constraints and Opportunities. *Resources Policy* **2014**, *41*, 52–59. https://doi.org/10.1016/j.resourpol.2014.03.004.

(7) Binnemans, K.; Jones, P. T.; Blanpain, B.; Van Gerven, T.; Pontikes, Y. Towards Zero-Waste Valorisation of Rare-Earth-Containing Industrial Process Residues: A Critical Review. *Journal of Cleaner Production* **2015**, *99*, 17–38. https://doi.org/10.1016/j.jclepro.2015.02.089.

(8) Kabata-Pendias, A. *Trace Elements in Soils and Plants*, 4th ed.; CRC Press: Boca Raton, 2011.

(9) Abhilash; Sinha, S.; Sinha, M. K.; Pandey, B. D. Extraction of Lanthanum and Cerium from Indian Red Mud. *International Journal of Mineral Processing* **2014**, *127*, 70–73. https://doi.org/10.1016/j.minpro.2013.12.009.

(10) Ochsenkühn-Petropoulou, M. Th.; Hatzilyberis, K. S.; Mendrinos, L. N.; Salmas, C. E. Pilot-Plant Investigation of the Leaching Process for the Recovery of Scandium from Red Mud. *Ind. Eng. Chem. Res.* **2002**, *41* (23), 5794–5801. https://doi.org/10.1021/ie011047b.

(11) Borra, C. R.; Pontikes, Y.; Binnemans, K.; Van Gerven, T. Leaching of Rare Earths from Bauxite Residue (Red Mud). *Minerals Engineering* **2015**, *76*, 20–27. https://doi.org/10.1016/j.mineng.2015.01.005.

(12) Qu, Y.; Lian, B. Bioleaching of Rare Earth and Radioactive Elements from Red Mud Using Penicillium Tricolor RM-10. *Bioresource Technology* **2013**, *136*, 16–23. https://doi.org/10.1016/j.biortech.2013.03.070.

(13) Borra, C. R.; Blanpain, B.; Pontikes, Y.; Binnemans, K.; Van Gerven, T. Recovery of Rare Earths and Other Valuable Metals From Bauxite Residue (Red Mud): A Review. *J. Sustain. Metall.* **2016**, *2* (4), 365–386. https://doi.org/10.1007/s40831-016-0068-2.

(14) Ravel, B.; Newville, M. ATHENA, ARTEMIS, HEPHAESTUS: Data Analysis for X-Ray Absorption Spectroscopy Using IFEFFIT. *J Synchrotron Rad* **2005**, *12* (4), 537–541. https://doi.org/10.1107/S0909049505012719.

(15) Doelsch, E.; Basile-Doelsch, I.; Rose, J.; Masion, A.; Borschneck, D.; Hazemann, J.-L.; Saint-Macary, H.; Bottero, J.-Y. New Combination of EXAFS Spectroscopy and Density Fractionation for the Speciation of Chromium within an Andosol. *Environ. Sci. Technol.* **2006**, *40* (24), 7602–7608. https://doi.org/10.1021/es060906q.

(16) Vind, J.; Malfliet, A.; Blanpain, B.; Tsakiridis, P.; Tkaczyk, A.; Vassiliadou, V.; Panias, D. Rare Earth Element Phases in Bauxite Residue. *Minerals* **2018**, *8* (2), 77. https://doi.org/10.3390/min8020077.

(17) Gräfe, M.; Power, G.; Klauber, C. Bauxite Residue Issues: III. Alkalinity and Associated Chemistry. *Hydrometallurgy* **2011**, *108* (1–2), 60–79. https://doi.org/10.1016/j.hydromet.2011.02.004.
(18) Cusack, P. B.; Courtney, R.; Healy, M. G.; O' Donoghue, L. M. T.; Ujaczki, É. An Evaluation of the General Composition and Critical Raw Material Content of Bauxite Residue in a Storage Area over a Twelve-Year Period. *Journal of Cleaner Production* **2019**, *208*, 393–401. https://doi.org/10.1016/j.jclepro.2018.10.083.
(19) Xue, S.; Zhu, F.; Kong, X.; Wu, C.; Huang, L.; Huang, N.; Hartley, W. A Review of the Characterization and Revegetation of Bauxite Residues (Red Mud). *Environ Sci Pollut Res* **2016**, *23* (2), 1120–1132. https://doi.org/10.1007/s11356-015-4558-8.
(20) Snars, K.; Gilkes, R. J. Evaluation of Bauxite Residues (Red Muds) of Different Origins for Environmental Applications. *Applied Clay Science* **2009**, *46* (1), 13–20. https://doi.org/10.1016/j.clay.2009.06.014.
(21) Atasoy, A. An Investigation on Characterization and Thermal Analysis of the Aughinish Red Mud. *J Therm Anal Calorim* **2005**, *81* (2), 357–361. https://doi.org/10.1007/s10973-005-0792-5.
(22) Samal, S.; Ray, A. K.; Bandopadhyay, A. Proposal for Resources, Utilization and Processes of Red Mud in India — A Review. *International Journal of Mineral Processing* **2013**, *118*, 43–55. https://doi.org/10.1016/j.minpro.2012.11.001.
(23) Goyne, K. W.; Brantley, S. L.; Chorover, J. Rare Earth Element Release from Phosphate Minerals in the Presence of Organic Acids. *Chemical Geology* **2010**, *278* (1–2), 1–14. https://doi.org/10.1016/j.chemgeo.2010.03.011.
(24) Brisson, V. L.; Zhuang, W.-Q.; Alvarez-Cohen, L. Bioleaching of Rare Earth Elements from Monazite Sand: Bioleaching of Rare Earth Elements from Monazite. *Biotechnol. Bioeng.* **2016**, *113* (2), 339–348. https://doi.org/10.1002/bit.25823.
(25) Shan, X.; Wang, H.; Zhang, S.; Zhou, H.; Zheng, Y.; Yu, H.; Wen, B. Accumulation and Uptake of Light Rare Earth Elements in a Hyperaccumulator Dicropteris Dichotoma. *Plant Science* **2003**, *165* (6), 1343–1353. https://doi.org/10.1016/S0168-9452(03)00361-3.
(26) Chi, R.; Xu, Z. A Solution Chemistry Approach to the Study of Rare Earth Element Precipitation by Oxalic Acid. *Metall and Materi Trans B* **1999**, *30* (2), 189–195. https://doi.org/10.1007/s11663-999-0047-0.
(27) Khawassek, Y. M. Adsorption of Rare Earth Elements by Strong Acid Cation Exchange Resin Thermodynamics, Characteristics and Kinetics. 11.
(28) Silva, R. G.; Morais, C. A.; Teixeira, L. V.; Oliveira, É. D. Selective Precipitation of High-Quality Rare Earth Oxalates or Carbonates from a Purified Sulfuric Liquor Containing Soluble Impurities. *Mining, Metallurgy & Exploration* **2019**, *36* (5), 967–977. https://doi.org/10.1007/s42461-019-0090-6.
(29) Jorjani, E.; Shahbazi, M. The Production of Rare Earth Elements Group via Tributyl Phosphate Extraction and Precipitation Stripping Using Oxalic Acid. *Arabian Journal of Chemistry* **2016**, *9*, S1532–S1539. https://doi.org/10.1016/j.arabjc.2012.04.002.
(30) Smith, R. M.; Martell, A. E. *Critical Stability Constants*; Springer US: Boston, MA, 1989. https://doi.org/10.1007/978-1-4615-6764-6.
(31) Martell, A. E.; Smith, R. M. *Other Organic Ligands*; Springer US: Boston, MA, 1977. https://doi.org/10.1007/978-1-4757-1568-2.
(32) Ochsenkühn-Petropulu, M.; Lyberopulu, Th.; Ochsenkühn, K. M.; Parissakis, G. Recovery of Lanthanides and Yttrium from Red Mud by Selective Leaching. *Analytica Chimica Acta* **1996**, *319* (1–2), 249–254. https://doi.org/10.1016/0003-2670(95)00486-6.

(33) Liu, X.; Byrne, R. H. Rare Earth and Yttrium Phosphate Solubilities in Aqueous Solution. *Geochimica et Cosmochimica Acta* **1997**, *61* (8), 1625–1633. https://doi.org/10.1016/S0016-7037(97)00037-9.
(34) Li, X.-Z.; Zhou, L.-P.; Yan, L.-L.; Dong, Y.-M.; Bai, Z.-L.; Sun, X.-Q.; Diwu, J.; Wang, S.; Bünzli, J.-C.; Sun, Q.-F. A Supramolecular Lanthanide Separation Approach Based on Multivalent Cooperative Enhancement of Metal Ion Selectivity. *Nat Commun* **2018**, *9* (1), 547. https://doi.org/10.1038/s41467-018-02940-7.
(35) Deblonde, G. J.-P.; Mattocks, J. A.; Park, D. M.; Reed, D. W.; Cotruvo, J. A.; Jiao, Y. Selective and Efficient Biomacromolecular Extraction of Rare-Earth Elements Using Lanmodulin. *Inorg. Chem.* **2020**, *59* (17), 11855–11867. https://doi.org/10.1021/acs.inorgchem.0c01303.
(36) Cotruvo, J. A.; Featherston, E. R.; Mattocks, J. A.; Ho, J. V.; Laremore, T. N. Lanmodulin: A Highly Selective Lanthanide-Binding Protein from a Lanthanide-Utilizing Bacterium. *J. Am. Chem. Soc.* **2018**, *140* (44), 15056–15061. https://doi.org/10.1021/jacs.8b09842.
(37) Bau, M.; Tepe, N.; Mohwinkel, D. Siderophore-Promoted Transfer of Rare Earth Elements and Iron from Volcanic Ash into Glacial Meltwater, River and Ocean Water. *Earth and Planetary Science Letters* **2013**, *364*, 30–36. https://doi.org/10.1016/j.epsl.2013.01.002.
(38) Christenson, E. A.; Schijf, J. Stability of YREE Complexes with the Trihydroxamate Siderophore Desferrioxamine B at Seawater Ionic Strength. *Geochimica et Cosmochimica Acta* **2011**, *75* (22), 7047–7062. https://doi.org/10.1016/j.gca.2011.09.022.
(39) Kraemer, D.; Kopf, S.; Bau, M. Oxidative Mobilization of Cerium and Uranium and Enhanced Release of "Immobile" High Field Strength Elements from Igneous Rocks in the Presence of the Biogenic Siderophore Desferrioxamine B. *Geochimica et Cosmochimica Acta* **2015**, *165*, 263–279. https://doi.org/10.1016/j.gca.2015.05.046.
(40) Canarini, A.; Kaiser, C.; Merchant, A.; Richter, A.; Wanek, W. Root Exudation of Primary Metabolites: Mechanisms and Their Roles in Plant Responses to Environmental Stimuli. *Front. Plant Sci.* **2019**, *10*, 157. https://doi.org/10.3389/fpls.2019.00157.
(41) Fathollahzadeh, H. Role of Microorganisms in Bioleaching of Rare Earth Elements from Primary and Secondary Resources. *Appl Microbiol Biotechnol* **2019**, 15.
(42) Mowafy, A. M. Biological Leaching of Rare Earth Elements. *World J Microbiol Biotechnol* **2020**, *36* (4), 61. https://doi.org/10.1007/s11274-020-02838-x.
(43) Liu, C.; Sun, D.; Zheng, H.-X.; Wang, G.-B.; Liu, W.-S.; Cao, Y.; Tang, Y.-T.; Qiu, R.-L. The Limited Exclusion and Efficient Translocation Mediated by Organic Acids Contribute to Rare Earth Element Hyperaccumulation in Phytolacca Americana. *Science of The Total Environment* **2022**, *805*, 150335. https://doi.org/10.1016/j.scitotenv.2021.150335.
(44) Clarholm, M.; Skyllberg, U.; Rosling, A. Organic Acid Induced Release of Nutrients from Metal-Stabilized Soil Organic Matter – The Unbutton Model. *Soil Biology and Biochemistry* **2015**, *84*, 168–176. https://doi.org/10.1016/j.soilbio.2015.02.019.
(45) Mattocks, J. A.; Cotruvo, J. A. Biological, Biomolecular, and Bio-Inspired Strategies for Detection, Extraction, and Separations of Lanthanides and Actinides. *Chem. Soc. Rev.* **2020**, *49* (22), 8315–8334. https://doi.org/10.1039/D0CS00653J.
(46) Osman, Y.; Gebreil, A.; Mowafy, A. M.; Anan, T. I.; Hamed, S. M. Characterization of Aspergillus Niger Siderophore That Mediates Bioleaching of Rare Earth Elements from Phosphorites. *World J Microbiol Biotechnol* **2019**, *35* (6), 93. https://doi.org/10.1007/s11274-019-2666-1.

(47) Macías-Pérez, L. A.; Levard, C.; Barakat, M.; Angeletti, B.; Borschneck, D.; Poizat, L.; Achouak, W.; Auffan, M. Contrasted Microbial Community Colonization of a Bauxite Residue Deposit Marked by a Complex Geochemical Context. *Journal of Hazardous Materials* **2022**, *424*, 127470. https://doi.org/10.1016/j.jhazmat.2021.127470.
(48) Fourrier, C.; Luglia, M.; Hennebert, P.; Foulon, J.; Ambrosi, J.-P.; Angeletti, B.; Keller, C.; Criquet, S. Effects of Increasing Concentrations of Unamended and Gypsum Modified Bauxite Residues on Soil Microbial Community Functions and Structure – A Mesocosm Study. *Ecotoxicology and Environmental Safety* **2020**, *201*, 110847. https://doi.org/10.1016/j.ecoenv.2020.110847.
(49) Fourrier, C.; Luglia, M.; Keller, C.; Hennebert, P.; Foulon, J.; Ambrosi, J.-P.; Angeletti, B.; Criquet, S. How Raw and Gypsum Modified Bauxite Residues Affect Seed Germination, Enzyme Activities, and Root Development of Sinapis Alba. *Water Air Soil Pollut* **2021**, *232* (8), 309. https://doi.org/10.1007/s11270-021-05232-x.

For Table of Contents Use Only